ACS APPLIED MATERIALS & INTERFACES

Research Article

www.acsami.org

Complementary Charge Trapping and Ionic Migration in Resistive Switching of Rare-Earth Manganite $TbMnO_3$

Yimin Cui,[†] Haiyang Peng,[‡] Shuxiang Wu,[‡] Rongming Wang,*[,†] and Tom Wu*[,‡]

[†]Key Laboratory of Micro-nano Measurement-Manipulation and Physics (Ministry of Education), Department of Physics, Beihang University, Beijing 100191, China

[‡]Division of Physics and Applied Physics, School of Physical and Mathematical Sciences, Nanyang Technological University, Singapore 637371, Singapore

ABSTRACT: Perovskite rare-earth manganites like $TbMnO_3$ exhibit rich magnetic and electric phases, providing opportunities for next-generation multifunctional devices. Here, we report the nonvolatile bipolar switching of resistance and capacitance in $TbMnO_3$ thin films grown on conducting $Nb:SrTiO_3$ substrates. The device shows an ON/OFF resistance ratio of $\sim 1 \times 10^4$, and the resistive switching is accompanied by a frequency-dependent capacitance switching. Detailed analysis of the conduction mechanisms reveals that the migration of oxygen vacancies and the charge trapping/detrapping at the heterojunction interface play important and complementary roles in the switching behaviors. Our results suggest that both electronic and ionic processes should be considered in order to elucidate the conduction mechanisms and the switching behaviors in such heterostructures made of complex oxides.

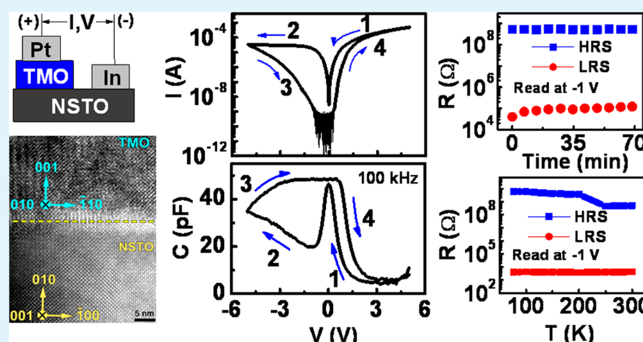

KEYWORDS: *$TbMnO_3$, resistive switching, capacitance switching, charge trapping, oxygen vacancies, ionic migration*

INTRODUCTION

Recently, nonvolatile random access memories based on resistive switching (RS) have attracted much attention due to their simple structure, good performance, and potential process compatibility with the conventional semiconductor technology.[1−9] Besides binary transition metal oxides and chalcogenides,[10−19] reliable RS has been observed in a variety of ternary complex oxides.[20−32] Such studies enrich the research of RS because the emergent physics in complex oxides based on correlated charge, spin, orbital, and lattice degrees of freedoms can potentially lead to multifunctional devices. But the underlying mechanisms of RS remain controversial, often involving multiple crystallographic, chemical, and electronic transformations on the microscopic level.[3,33−35] In literature, the RS mechanisms usually belong to three categories: (1) thermochemical type where Joule heating causes the formation and rupture of localized conducting filaments; (2) electrochemical type where the cation migration leads to the formation and dissolution of metal filaments; and (3) valence change type where electric field induces the modulation of Schottky/tunneling barrier at the interface.[7] Among rare-earth manganites, $TbMnO_3$ (TMO) is one of the most notable perovskite oxides because of its remarkable multiferroic properties as a result of the unique spiral spin order.[36,37] Although much research has been done on the preparation and characterization of TMO single crystals and thin films,[36−40] there has been no report on RS in TMO-based devices.

In this work, we report the bipolar switching of resistance and capacitance in Pt/TMO/$Nb:SrTiO_3$ (NSTO) heterojunctions. The RS device shows reliable memory performance, and the capacitance switching is strongly frequency dependent. Detailed analysis of the conduction mechanisms reveals that migration of oxygen vacancies and trapping/detrapping of charges at the TMO/NSTO interface drive the switching behaviors. Different from the usually cited RS mechanisms involving localized conducting filaments or modified Schottky/tunneling barriers, our data suggest that both ionic and electronic processes play important roles in the transport of Pt/TMO/NSTO heterostructures, producing complementary effects. Our results open doors toward future explorations of switching behaviors in a wide range of rare earth manganites with multiple coupled degrees of freedom.

EXPERIMENTAL SECTION

To prepare the heterojunctions, we grown 50 nm TMO thin films on NSTO (100) (0.7 wt % Nb doping) single-crystal substrates at 720 °C using pulsed laser deposition. The details of the film preparation were described in previous works.[39] The X-ray diffraction (XRD) data in Figure 1a indicates that the *c*-axis oriented TMO film were epitaxially grown on the (001) NSTO substrate. Figure 1b shows the high resolution transmission electron microscopy (HRTEM) image

Received: August 24, 2012
Accepted: January 23, 2013
Published: January 23, 2013

 © 2013 American Chemical Society

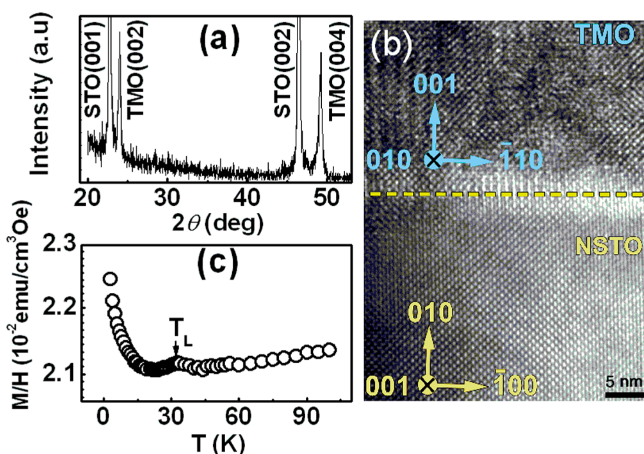

Figure 1. (a) XRD pattern of the *c*-axis oriented TMO film grown on (001) NSTO. (b) High-resolution cross-section TEM image obtained near the TMO/NSTO interface. (c) Magnetization vs temperature plot of the TMO film measured under the zero-field cooled condition, and the arrow marks the lock-in temperature.

obtained at the TMO/NSTO interface, indicating a coherent growth. Figure 1c shows the magnetization versus temperature curve of the TMO film measured under the zero-field-cooled condition with a magnetic field of 200 Oe. The anomalous feature at ∼32 K is reminiscent of the lock-in temperature T_L reported in TMO single crystals, which is a result of the incommensurate-commensurate transition of the magnetic modulation wave vector.[36] This characteristics temperature in the TMO thin film is slightly higher than that of the bulk counterpart (28 K); the reason is unknown at the moment, but it may be related to the finite size effect in thin films.

To fabricate the RS devices, we deposited Pt top electrodes with areas of 0.01 to 0.25 mm^2 on the TMO thin films by sputtering through a shadow mask, and In metal serves as the bottom electrode on the NSTO substrate. The schematic of the Pt/TMO/NSTO/In device is illustrated in the left inset of Figure 2a. A positive voltage bias applied to the devices is defined as the current flowing from the Pt electrode into the TMO layer.

RESULTS AND DISCUSSION

The current−voltage ($I-V$) curves of the pristine devices show the typical rectifying characteristics. After the junction was electrically stressed by voltage pulses (typically, 8 V for 5 s), bipolar RS can be reliably observed. As shown in Figure 2a, a sweep of positive bias switches the device into a low resistance state (LRS), whereas a subsequent reverse sweep drives it back to the high resistance state (HRS). The 100 cycles in Figure 2a show steady and reproducible operations. The ON/OFF ratio read at −1 V is nearly 1×10^4, which is satisfactory for nonvolatile memory applications. As a reference, we measured the $I-V$ curve of a Pt/TMO/$YBa_2Cu_3O_{7-x}$ (YBCO) device where YBCO serves as a highly conducting electrode, and the clearly observed ohmic behavior (right inset of Figure 2a) suggests that the Pt/TMO junction does not present a dominant resistance with rectification. Furthermore, the In/NSTO is ohmic because of the metallic characteristics of both In and NSTO. Thus we can conclude that the observed RS behavior is an intrinsic property of the TMO/NSTO junction.

The devices exhibit data retention within the measurement period when the ON/OFF states were repeatedly read at −1 V (Figure 2b). We observed a slight increase of the LRS with repeated read operations, but the ON/OFF ratio remains larger than 1×10^3. Furthermore, the HRS resistance appears to increase as the electrode area decreases (Figure 2 c), indicating

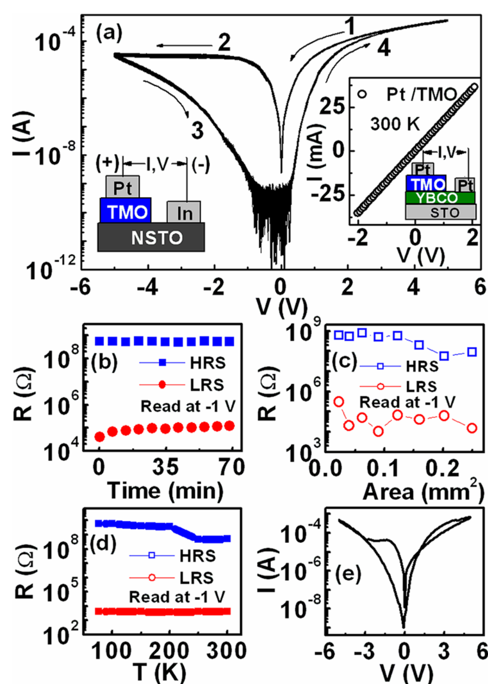

Figure 2. (a) $I-V$ characteristics of the Pt/TMO/NSTO device plotted in semilog scale. The overlapped 100 consecutive sweeping cycles indicate excellent operating endurance. The left inset is a schematic of the device, and the right inset is the $I-V$ characteristics of the reference Pt/TMO/YBCO device. (b) Retention data of the device. (c) Electrode area dependence of HRS and LRS resistance. (d) Temperature dependence of HRS and LRS resistance. (e) $I-V$ characteristics of the device annealed in oxygen ambient at 700 °C for 20 min.

that the switching mechanism is interface related. But the trend of area dependence of the LRS is less clear with substantial data fluctuation. It is likely that the perpendicular-to-plane transport across the TMO heterostructure is not homogeneous, and structural defects may induce local enhancement of the leakage current.

We also examined the temperature dependence of the two resistance states. As shown in Figure 2d, the HRS resistance increases with decreasing temperature; the LRS exhibits a similar temperature-dependent trend, but the variation of resistance is much smaller. This indicates that the conduction of the LRS is not dominated by metallic filaments. Otherwise, the temperature-dependent resistance data should show a clear metal-like behavior.

To further shed light on the transport behavior, we annealed the device in oxygen ambient at 700 °C for 20 min and found that the $I-V$ hysteresis is reduced after annealing (Figure 2e). This stoichiometry-property correlation implies that oxygen vacancies likely play an important role in the RS operation of the Pt/TMO/NSTO heterostructures. It should be noted that we are not aware of any theoretical or experimental study on the defect characteristics in TMO thin films, and the formation energies of various possible defects are also unknown. A systematic investigation of the defect chemistry in Pt/TMO/NSTO heterostructures is out of the scope of this study. However, oxygen vacancies are the most likely defect because the environment in PLD growth is in general oxygen-poor with a reducing nature.

To shed light on the carrier dynamics, we carried out capacitance−voltage ($C-V$) measurements on the Pt/TMO/

dx.doi.org/10.1021/am301769f | ACS Appl. Mater. Interfaces 2013, 5, 1213−1217

NSTO device in a wide frequency range from 10 kHz to 4 MHz. As shown in Figure 3, prominent hysteresis was observed

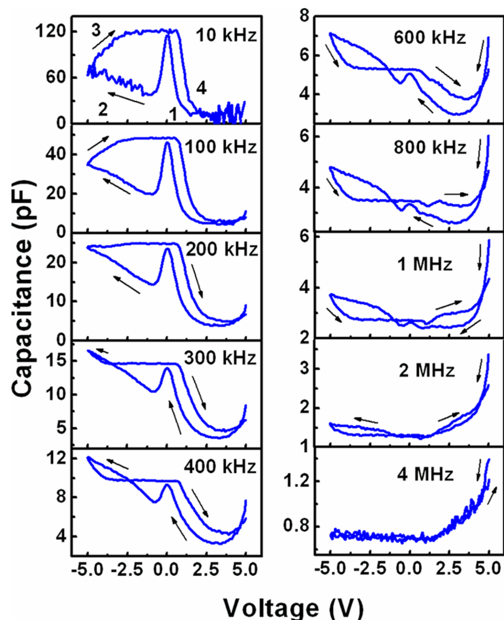

Figure 3. $C-V$ loops of the Pt/TMO/NSTO device measured in a frequency range of 10 k to 4 MHz.

at low frequencies in the range of 10−200 kHz, which is gradually suppressed at higher frequencies and the magnitude drops to the level of a few pF when the frequency increases to the MHz level. This notable frequency-dependent hysteretic behavior is characteristic of Schottky or p−n junctions with deep impurity levels.[41,42]

The $C-V$ data help to shed light on the switching dynamics of the TMO/NSTO heterojunction. Applying voltage biases can drive the migration of both charged carriers and ionic defects,[35] and the modulation of the depletion layer plays pivotal roles in both the resistance and the capacitance switching. We can exclude the formation and rupture of conducting filaments as the dominant switching mechanism because the metallic filamentary conduction would lead to inductor-like response and prevent the reliable capacitance measurements. This is also consistent with the temperature dependent resistance measurement data in Figure 2d, where we did not observe a metal-like behavior in the LRS. In the TMO/NSTO junction, the capacitance is determined by the displacement current of the charged carriers through the depletion layer. This explains the strong frequency dependence: If the measurement frequency is very high, then the charges and defects cannot respond to the electric field due to their finite time of relaxation,[42,43] leading to the suppressed capacitance as observed in Figure 3.

To get further insight on the RS at the TMO/NSTO interface, we examined in detail the conduction mechanisms of the four $I-V$ branches in Figure 2a. Figure 4a shows the log−log plot of branch 1 (LRS, positive bias), and the slope of the linear fitting curve is close to 2, which suggests the space-charge-limited (SCL) conduction mechanism. In this bulk-limited mechanism, the transport follows the Child's law[44]

$$I_{\mathrm{SCL}} = \frac{9A\varepsilon_{\mathrm{r}}\varepsilon_0\mu V^2}{8d^3} \quad (1)$$

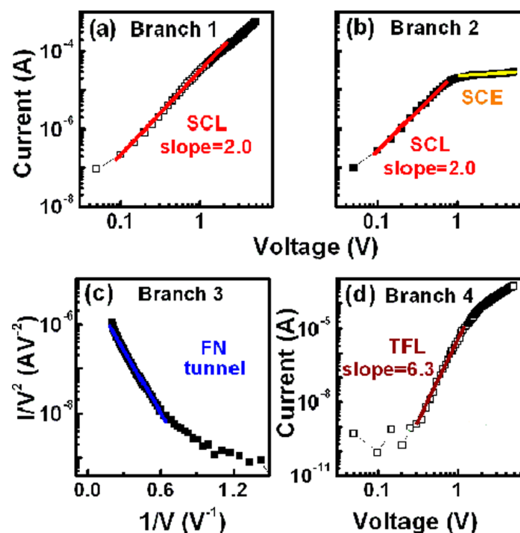

Figure 4. Replots of the four $I-V$ branches in Figure 2a along with fittings to various conduction mechanisms, i.e., (a, b) SCL conduction in the LRS branches; (c) F−N tunneling at high voltages in the HRS branch; (d) TFL conduction in the intermediate voltage region.

where A is junction area, I is the current density, V is the bias voltage, μ is the mobility of the charge carriers, ε_r is the relative dielectric constant, ε_0 is the permittivity of free space, and d is the film thickness. This indicates that within the measured voltage range the injected excess carriers, instead of the intrinsic thermally generated carriers in TMO, dominate the transport. The SCL conduction mechanism is quite common in oxides with high-density defects and charge traps, and it was reported previously in junctions based on complex oxides.[45−47] Using eq 1 and the dielectric constant ε_r of TMO film (about 200 at 300 K),[48] the carrier mobility of TMO can be calculated as 3.1×10^{-6} cm^2/(V s). This derived low mobility is consistent with the insulator nature of TMO. Figure 4b shows the log−log plot of branch 2 (LRS, negative bias), and the conduction mechanism is still SCL when voltage is low than 0.9 V, whereas the current saturates at higher voltages because of the stored-charge effect (SCE).[49]

In branch 3 (HRS, negative bias), the current decreases sharply as the voltage goes down. There are three common mechanisms to account for the leakage current under a high voltage bias: Schottky emission,[50] Poole−Frenkel emission,[51] and Fowler−Nordheim (F−N) tunneling.[52] In the Schottky emission, the $I-V$ curve obeys the relationship of $\ln I \propto V^{1/2}$, which does not fit the data. We found that the Poole−Frenkel emission cannot explain the $I-V$ curve either. As shown in Figure 4c, at voltages higher than ∼1.5 V, the conduction follows the behavior of F−N tunneling[52]

$$I_{\mathrm{FN}} = \frac{ABV^2}{d^2}\exp\left(-\frac{dC\phi_{\mathrm{i}}^{3/2}}{V}\right) \quad (2)$$

where B and C are material-dependent constants and ϕ_i is the potential barrier height. It implies that at the high electric field, electrons may tunnel from the cathode into the conduction band of TMO layer. This scenario is consistent with the very weak temperature dependence of resistance of the HRS near room temperature. Furthermore, with the assumptions of triangular barrier and WKB approximation for the tunneling probability, the constant C can be written as $4(2m)^{1/2}/3\hbar q$,

dx.doi.org/10.1021/am301769f | ACS Appl. Mater. Interfaces 2013, 5, 1213−1217

where m is the free-electron mass, $\hbar$ is the Plank's constant, and q is the electronic charge.[53] In the Fowler–Nordheim plot ($\log I/V^2$ vs $1/V$), the potential barrier ϕ_i can be estimated as ~1.1 eV, which is consistent with the previously reported result.[54]

Finally, the branch 4 (HRS, positive bias) in Figure 4d is dominated by a sharp current increase with a slope of ~6.3. The sharp increase in the leakage current occurs at the so-called trap-filled-limit (TFL) voltage (V_{TFL}), which can be expressed as[44]

$$V_{TFL} = \frac{8qd^2N_t}{9\varepsilon_r\varepsilon_0} \tag{3}$$

where N_t is the trapped electron density. After the traps are filled, the conduction recovers its trap-free characteristics (branch 1 in Figure 4a). The trap-related mechanism is consistent with the annealing result (Figure 2e): Because annealing can effectively eliminate these traps, the RS characteristics are reduced in the annealed samples.

The overall resistance and capacitance switching behaviors of the TMO/NSTO junction can be understood by considering the trapping/detrapping of charge carriers and the dynamic migration of oxygen vacancies in the depletion layer at the TMO/NSTO interface. Because the carrier concentration of TMO is much lower than that of NSTO, the depletion layer is mainly at the TMO side. Positively charged oxygen vacancies and their complexes can serve as traps for charged carriers at the TMO/NSTO interface. In the branch 1 of the $I-V$ loops, lots of electrons flowing from the n-type NSTO get trapped, giving rise to a high leakage current at the high forward bias and the SCL conduction, at the same time the excessive leakage current at the high voltage leads to a low capacitance. Consequently, in the branch 2, as the voltage sweeps to the negative side, the polarity of both voltage and current is reversed. When the Pt electrode is negative biased, the positively charged oxygen vacancies are removed from the interface region; as a consequence, the defect density and the leakage current at the interface are reduced, and the device is reset to the HRS in the branch 3. Concomitantly, there are less leaky current across the heterojunction, which gives rise to a high capacitance. The branch 4 accomplishes the transition from HRS to LRS, and the steep current increase is a result of rapidly filled traps, simultaneously leading to a low capacitance at the high bias. The sweep of positive voltage moves the oxygen vacancies into the interface region, which leads to the trapping-dominated transport and sets the device to LRS. Overall, the current under the positive bias (branches 1 and 4) is notably higher than that under the negative bias (branches 2 and 3) because the conducting NSTO substrate is strongly n-type with carrier concentration much higher than that of the TMO layer. Our experiments suggest that the TMO/NSTO heterostructure behaves as a switchable diode, which is promising to present more functionalities in future studies. Furthermore, both the electronic SCL conduction and the ionic vacancy migration are indispensable ingredients in the data interpretation, producing complementary effects in the device operation.

CONCLUSION

In summary, we have demonstrated reliable bipolar resistance and capacitance switching in the TMO/NSTO junctions. The ON/OFF ratio of the RS device reaches $\sim 1 \times 10^4$, which is accompanied by data retention and operation endurance. Furthermore, the junction capacitance exhibits clear hysteresis loops in voltage sweeps and strong frequency dependence. These behaviors can be attributed to the dynamic and complementary electronic trapping/detrapping and ionic defect migration at the junction interface. The observed rich switching behaviors make TMO a versatile candidate to construct multifunctional devices, and may open new doors toward manipulating the rich properties of such rare earth manganites. We also expect that such switching behaviors may be general in other rare-earth manganites and their epitaxial heterostructures.

AUTHOR INFORMATION

Corresponding Author

*E-mail: tomwu@ntu.edu.sg; rmwang@buaa.edu.cn.

Notes

The authors declare no competing financial interest.

ACKNOWLEDGMENTS

We acknowledge the supports from the National Natural Science Foundation of China (10975013) and the National Research Foundation of Singapore.

REFERENCES

(1) Liu, S. Q.; Wu, N. J.; Ignatiev, A. *Appl. Phys. Lett.* **2000**, *76*, 2749.
(2) Beck, A.; Bednorz, J. G.; Gerber, C.; Rossel, C.; Widmer, D. *Appl. Phys. Lett.* **2000**, *77*, 139.
(3) Szot, K.; Speier, W.; Bihlmayer, G.; Waser, R. *Nat. Mater.* **2006**, *5*, 312–320.
(4) Waser, R.; Aono, M. *Nat. Mater.* **2007**, *6*, 833–840.
(5) Meijer, G. I. *Science* **2008**, *319*, 1625–1626.
(6) Strukov, D. B.; Snider, G. S.; Stewart, D. R.; Williams, R. S. *Nature* **2008**, *453*, 80–83.
(7) Waser, R.; Dittmann, R.; Staikov, G.; Szot, K. *Adv. Mater.* **2009**, *21*, 2632–2663.
(8) Nagashima, K.; Yanagida, T.; Oka, K.; Kawai, T. *Appl. Phys. Lett.* **2009**, *94*, 242902.
(9) Kim, K. M.; Jeong, D. S.; Hwang, C. S. *Nanotechnology* **2011**, *22*, 254002.
(10) Terabe, K.; Hasegawa, T.; Nakayama, T.; Aono, M. *Nature* **2005**, *433*, 47–50.
(11) Lee, M. J.; Lee, C. B.; Lee, D.; Lee, S. R.; Chang, M.; Hur, J. H.; Kim, Y. B.; Kim, C. J.; Seo, D. H.; Seo, S.; Chung, U. I.; Yoo, I. K.; Kim, K. *Nat. Mater.* **2011**, *10*, 625–630.
(12) Yang, J. J.; Miao, F.; Pickett, M. D.; Ohlberg, D. A. A.; Stewart, D. R.; Lau, C. N.; Williams, R. S. *Nanotechnology* **2009**, *21*, 215201.
(13) Lee, M. J.; Kim, S. I.; Lee, C. B.; Yin, H.; Ahn, S. E.; Kang, B. S.; Kim, K. H.; Park, J. C.; Kim, C. J.; Song, I.; Kim, S. W.; Stefanovich, G.; Lee, J. H.; Chung, S. J.; Kim, Y. H.; Park, Y. *Adv. Func. Mater* **2009**, *19*, 1587–1593.
(14) Shang, D. S.; Shi, L.; Sun, J. R.; Shen, B. G. *Nanotechnology* **2011**, *22*, 254008.
(15) Kim, G. H; Lee, J. H.; Seok, J. Y.; Song, S. J.; Yoon, J. H.; Yoon, K. J.; Lee, M. H.; Kim, K. M.; Lee, H. D.; Ryu, S. W.; Park, T. J.; Hwang, C. S. *Appl. Phys. Lett.* **2011**, *98*, 262901.
(16) Kwon, D. H.; Kim, K. M.; Jang, J. H.; Jeon, J. M.; Lee, M. H.; Kim, G. H.; Li, X. Shu.; Park, G. S.; Lee, B.; Han, S.; Kim, M.; Hwang, C. S. *Nat. Nanotechnol.* **2010**, *5*, 148–153.
(17) Peng, H. Y.; Li, Y. F.; Lin, W. N.; Wang, Y. Z.; Gao, X. Y.; Wu, T. *Sci. Rep.* **2012**, *2*, 442.
(18) Du, Y. M.; Pan, H.; Wang, S. J.; Wu, T.; Feng, Y. P.; Pan, J.; Wee, A. T. S. *ACS Nano* **2012**, *6*, 2517.
(19) Ye, J. Y.; Li, Y. Q.; Gao, J.; Peng, H. Y.; Wu, S. X.; Wu, T. *Appl. Phys. Lett.* **2010**, *97*, 132108.
(20) Sawa, A.; Fujii, T.; Kawasaki, M.; Tokura, Y. *Appl. Phys. Lett.* **2004**, *85*, 4073.

(21) Hasan, M.; Dong, R.; Choi, H. J.; Lee, D. S.; Seong, D. J.; Pyun, M. B.; Hwang, H. *Appl. Phys. Lett.* **2008**, *92*, 202102.
(22) Rebello, A.; Mahendiran, R. *Appl. Phys. Lett.* **2009**, *94*, 112107.
(23) Wang, C.; Jin, K.; Xu, Z. T.; Wang, L.; Ge, C.; Lu, H. B.; Guo, H. Z.; He, M.; Yang, G. Z. *Appl. Phys. Lett.* **2011**, *98*, 192901.
(24) Yan, X. B.; Xia, Y. D.; Xu, H. N.; Gao, X.; Li, H.; Li, T. R.; Yin, J.; Liu, Z. G. *Appl. Phys. Lett.* **2010**, *97*, 112101.
(25) Ni, M. C.; Guo, S. M.; Tian, H. F.; Zhao, Y. G.; Li, J. Q. *Appl. Phys. Lett.* **2007**, *91*, 183502.
(26) Wu, S. X.; Peng, H. Y.; Wu, T. *Appl. Phys. Lett.* **2011**, *98*, 093503.
(27) Yan, Z. B.; Li, S. Z.; Wang, K. F.; Liu, J. M. *Appl. Phys. Lett.* **2010**, *96*, 012103.
(28) Bogle1, K. A.; Bachhav, M. N.; Deo, M. S.; Valanoor, N.; Ogale, S. B. *Appl. Phys. Lett.* **2009**, *95*, 203502.
(29) Li, M.; Zhuge, F.; Zhu, X.; Yin, K.; Wang, J.; Liu, Y.; He, C.; Chen, B.; Li, R. W. *Nanotechnology* **2010**, *21*, 425202.
(30) Ruotolo, A.; Leung, C. W.; Lam, C. Y.; Cheng, W. F.; Wong, K. H. *Phys. Rev. B* **2008**, *77*, 233103.
(31) Peng, H.; Wu, T. *Appl. Phys. Lett.* **2009**, *95*, 152106.
(32) Thakare, V.; Xing, G. Z.; Peng, H. Y.; Rana, A.; Game, O.; Kumar, P. A.; Banpurkar, A.; Kolekar, Y.; Ghosh, K.; Wu, T.; Sharma, D. D.; Ogale, S. B. *Appl. Phys. Lett.* **2012**, *100*, 172412.
(33) Inoue, I. H.; Yasuda, S.; Akinaga, H.; Takagi, H. *Phys. Rev. B* **2008**, *77*, 035105.
(34) Sawa, A. *Mater. Today* **2008**, *11*, 28−36.
(35) Muenstermann, R.; Menke, T.; Dittmann, R.; Waser, R. *Adv. Mater.* **2010**, *22*, 4819−4822.
(36) Kimura, T.; Goto, T.; Shintani, H.; Ishizaka, K.; Arima, T.; Tokura, Y. *Nature* **2003**, *426*, 55−58.
(37) Yamasaki, Y.; Sagayama, H.; Abe, N.; Arima, T.; Sasai, K.; Matsuura, M.; Hirota, K.; Okuyama, D.; Noda, Y.; Tokura, Y. *Phys. Rev. Lett.* **2008**, *101*, 097204.
(38) Abe, N.; Taniguchi, K.; Ohtani, S.; Umetsu, H.; Arima, T. *Phys. Rev. B* **2009**, *80*, 020402(R).
(39) Cui, Y. M.; Wang, C. C.; Cao, B. S. *Solid State Commun.* **2005**, *133*, 641−645.
(40) Marti, X.; Skumryev, V.; Ferrater, C.; García-Cuenca, M. V.; Varela, M.; Sánchez, F.; Fontcuberta, J. *Appl. Phys. Lett.* **2010**, *96*, 222505.
(41) Rhoderic, E. H. *Metal-Semiconductor Contacts*; Clarendon Press: Oxford, U.K., 1978; pp 193−198.
(42) Crowell, C. R.; Nakano, K. *Solid-State Electron.* **1972**, *15*, 605.
(43) Zhao, N.; Marinov, O.; Botton, G. A.; Deen, M. J.; Ong, B. S.; Wu, Y.; Liu, P. *IEEE Trans. Electron Devices* **2005**, *52*, 2150−2156.
(44) Lampert, M. A. *Phys. Rev.* **1956**, *103*, 1648−1656.
(45) Yang, H.; Wang, Y. Q.; Wang, H.; Jia, Q. X. *Appl. Phys. Lett.* **2010**, *96*, 012909.
(46) Wang, S. Y.; Cheng, B. L.; Wang, C.; Dai, S. Y.; Lu, H. B.; Zhou, Y. L.; Chen, Z. H.; Yang, G. Z. *Appl. Phys. Lett.* **2004**, *84*, 4116.
(47) Odagawa, A.; Sato, H.; Inoue, I. H.; Akoh, H.; Kawasaki, M.; Tokura, Y.; Kanno, T.; Adachi, H. *Phys. Rev. B* **2004**, *70*, 224403.
(48) Cui, Y. M.; Cai, W.; LI, Y.; Qian, J. Q.; Xu, P.; Wang, R. M.; Yao, J. E. *J. Appl. Phys.* **2006**, *100*, 034101.
(49) Dimitrijev, S. *Principles of Semiconductors Devices*; Oxford University Press: Oxfordm U.K., 2006; p 228.
(50) Schottky, W. *Naturwiss.* **1938**, *26*, 843.
(51) Frenkel, J. *Tech. Phys. USSR* **1938**, *5*, 685.
(52) Fowler, R. H.; Nordheim, L. W. *Proc. R. Soc. London, Ser. A* **1928**, *119*, 173−181.
(53) Lenzlinger, M.; Snow, E. H. *J. Appl. Phys.* **1969**, *40*, 278.
(54) Cui, Y. M.; Tian, Y. F.; Liu, W.; Li, Y. F.; Wang, R. M.; Wu, T. *AIP Adv.* **2011**, *1*, 042129.